Available online at www.sciencedirect.com

jmr&t Journal of Materials Research and Technology

journal homepage: www.elsevier.com/locate/jmrt

Original Article

Effect of bonding temperature and bonding time on microstructure of dissimilar transient liquid phase bonding of GTD111/BNi-2/IN718 system

Ali Izadi Ghahferokhi [a], *Masoud Kasiri-Asgarani* [a,**], *Reza Ebrahimi-kahrizsangi* [a], *Mahdi Rafiei* [a], *Hamid Reza Bakhsheshi-Rad* [a,*], *Kamran Amini* [b], *Filippo Berto* [c,***]

[a] *Advanced Materials Research Center, Department of Materials Engineering, Najafabad Branch, Islamic Azad University, Najafabad, Iran*

[b] *Department of Mechanical Engineering, Khomeinishahr Branch, Islamic Azad University, Khomeinishahr/Isfahan, Iran*

[c] *Department of Mechanical and Industrial Engineering, Norwegian University of Science and Technology, 7491 Trondheim, Norway*

ARTICLE INFO

Article history:
Received 5 July 2022
Accepted 6 October 2022
Available online 14 October 2022

Keywords:
Bonding temperature
Bonding time
Transient liquid phase bonding
Ni-based superalloy
BNi-2

ABSTRACT

The effect of bonding temperature and bonding time on the microstructure of transient liquid phase (TLP) bonding named GTD111 and IN718 superalloys, using a commercial Ni–B–Cr filler alloy (BNi-2) interlayer were evaluated. The sandwich assembly was kept in a vacuum furnace at temperatures of 1050, 1100, and 1150 °C for 1, 15, 30, 45, 60, and 80 min until the TLP process occurred. Microstructural characterization was carried out via optical microscopy, scanning electron microscopy (SEM) equipped with field emission energy dispersive spectroscopy (EDS), and X-ray diffraction (XRD). Microstructural assessments displayed those in little bonding times, the joint microstructure includes continuous eutectic intermetallic phases and longer times cause eutectic free microstructure. The bonding temperature affects the isothermal solidification rate, while, at low bonding temperatures microstructure of the joint centerline is controlled by diffusion of melting point depressant (MPD) elements. Despite, at high bonding temperature effect of base metal alloying elements on the joint microstructure development was more marked. The results showed that athermally solidified zone (ASZ) size reduces with increasing bonding temperature and time due to diffusion of boron into the base metal.

* Corresponding author.
** Corresponding author.
*** Corresponding author.
E-mail addresses: m.kasiri.a@gmail.com (M. Kasiri-Asgarani), reza.bakhsheshi@pmt.iaun.ac.ir (H.R. Bakhsheshi-Rad), filippo.berto@ntnu.no (F. Berto).

https://doi.org/10.1016/j.jmrt.2022.10.014

1. Introduction

Transient liquid phase (TLP) bonding is a process for the combination of benefits in diffusion welding and brazing. This process is the favored post-service joining/repairing method for Ni-based superalloys owing to its ability to produce near-ideal bonds [1]. The bonding of materials with low weldability employing a filler alloy with a melting point lower than the substrate and specific chemical composition could be done using the TLP process [2]. TLP bonding was used for materials that are difficult to joint by other processes. One of these materials that are difficult to joint by fusion welding is the Ni-based superalloys. The joining and welding are essential issues in the successful manufacture and cost-effectiveness of hot section components of power generation turbines and aircraft made from Ni-based superalloys. The prevention of the formation of uninvited intermetallic phases in the bond centreline is the critical key microstructural requirement in the joining of superalloys [3]. During brazing and fusion welding, unfavorable intermetallic phases are formed while cooling the liquid phase due to segregation induced by non-equilibrium solidification [4–7]. TLP bonding is considered as an attractive joining/repairing process for Ni-based superalloys as a result of producing an intermetallic free joint centreline through isothermal solidification [8–12].

Ni-based superalloys also attract considerable interest in the field of TLP due to their excellent mechanical performance for high-temperature applications and the difficulties of machining complex-geometry components. The principal reason for using the Ni-based superalloys in severe service and critical conditions is their stability with complex and multi-phase microstructures at high temperatures. Superalloys bonding temperature differs between 1000 and 1200 °C depending on the amount and the type of MPD elements as well as the existence of alloying elements in interlayer [4].

The Ni-based superalloy GTD111 is used in critical conditions such as manufacturing the first stage blades of powerful gas turbines that require corrosion, fatigue and creep properties under 70,000 h [13]. The GTD111, as a Ni-based superalloy material, was designed in the 1970s and utilized in the 1980s in high-power industrial gas turbines as the first stage blades. With the modification of IN738LC and Rene 80 could achieve to GTD111 with excellent high-temperature properties. The existence of refractory elements, for instance, Mo, W, Ta, Cr, and Co, prevents creep strength and local hot corrosion [14,15]. For the GTD111 superalloys, a higher strength joint can be made using this method in comparison to welding. The regularly accepted cause for this is that the welding of a GTD111 superalloy can lead to hot cracking and micro-fissuring through fusion welding [16]. Transient liquid phase bonding was developed for utilization in joining hot cracking sensitive Ni-based cast superalloys. It is cited as "TLP bonding" or "Activated diffusion bonding" [17]. IN718 is a Ni-based superalloy material originated by the International Nickel Company in the 50s [18]. This alloy is the Nb-modified Ni-Fe-based superalloy and has been broadly used in gas turbines and related applications because of its interest in structural stability, mechanical properties such as high strength, good formability, excellent ductility, and weldability at high temperatures [19].

Taking into consideration its broad application in different industries, the coupling of IN718 is an essential issue [20,21]. While the slow kinetics of γ'' precipitation prepares IN718 welds free of strain age cracking, the welding of IN718 takes pains from some problems, including [22]: liquation cracking and microfissuring in the heat-affected zone and separation of niobium during non-equilibrium solidification of the fusion zone and the following formation of the brittle niobium rich Laves phase [23–25].

The most important MPD elements in Ni-based filler alloys are boron, silicon, and phosphorous. The choice of filler alloy for a TLP bonded joint depends on many aspects, including filler metal melting properties and fluidity, design of joint, bonding time, requirements of service life (such as strength and corrosion resistance), base metal composition, and availability and cost. For instance, it has been announced that BNi-2 and BNi-3 filler alloys displayed good flow properties at low bonding temperatures, and BNi-9 is a great highly stressed component. The target of this study is to analyze and investigate the effects of bonding time and bonding temperature (in constant conditions) on microstructural features, with particular emphasis on the distribution of MPD elements and the time required for completion of isothermal solidification (t_{IS}) during TLP bonding of dissimilar Ni-based superalloys. In the previous studies, the effects of different parameters on the microstructure were investigated at one temperature and one time. The evolution of changes in the bonding temperatures and bonding times and their effects on the microstructure was reported in the current study [26,27].

In this study, the impacts of temperature and time on the microstructure of the transient liquid phase bonding (TLPB) of IN718 and GTD111 using Ni-B-Si interlayer were evaluated using optical microscopy scanning electron microscopy, and SEM/EDS analysis. The completion of isothermal solidification in TLP bonding of GTD111 and IN718 by use of BNi-2 interlayer at a temperature of 1050–1150 °C was surveyed. In addition, the bonding time effect at 1–80 min on microstructure development of diffusion affected zone and whole bonding zone was investigated.

2. Material and methods

In this study, various Ni-based superalloys that are GTD111 and IN718 were chosen and received in the form of a sheet of 5 mm thickness. The chemical composition of the GTD-111 nickel-base superalloy was Ni-13.5Cr-9.5Co-4.75Ti-3.3Al-3.8W-1.53Mo-2.7Ta-0.23Fe in term of wt.%. The chemical composition of IN718 nickel-base superalloy was Ni-18Cr-0.06Co-0.92Ti-0.4Al-4.41Nb-3.30Mo-0.05Ta-17.86Fe in term of wt.%. An interlayer with composition of Ni-7Cr-3Fe-4.5Si-3.2B and commerial name of BNi-2 in amorphous form and thickness of 75 mm was used as filler metal. The compositions of B-Ni interlayers such as BNi-2 filler metal in the form of amorphous foil with 50 μm thicknesses are also represented in Table 1. As specified, the joining metal parts were machined to dimensions of 10mm × 10mm × 5 mm using a wire cutting device. The joining facades were grounded using the grit sizes of No. 60–2000 SiC emery papers. The specimens were cleaned for 15 min in an acetone bath ultrasonically and

Table 1 – The EDS analysis (atomic %) of different areas in Fig. 3.

Elements	γ-solid solution	Ni-rich boride phase	Cr-rich boride	Ni-rich silicide
Ni	80.46	79.45	41.20	75.57
Cr	5.99	7.42	48.32	5.77
Fe	5.97	4.40	4.44	4.11
Nb	2.25	3.36	2.29	1.56
Ta	1.80	1.40	0.59	3.35
Si	0.64	1.21	0.24	7.77
Mo	1.22	2.14	0.80	0.06
Ti	1.53	0.45	1.70	1.71
Al	0.09	0.09	0.42	0.10

followed by the TLP bonding method in a vacuum furnace with the applied bonding pressure of 10^{-4} Torr. A schematic fixture for fixing the samples during the TLP bonding process is shown in Fig. 1.

The bonded specimens were prepared metallographically, and the sectioned specimens were ground using the grit sizes of No. 80–3000 SiC paper. The specimens were polished by disc polishing using Al_2O_3 suspension to reach a mirror surface of 1 μm on the joints. After metallographic preparation, the specimens were studied using optical (OM) and SEM equipped with EDS. The bonding was developed at 1050, 1100, and 1150 °C for 1–80 min. The heating rate was 10 °C/min, and it is then furnace-cooled to room temperature (the error measurement in the temperature is ± 5 °C). Two various etchants were used in order to study their microstructural properties. In order to show the precipitates adjacent to the interlayer/base metal interface, Murakami etchant (10g KOH, 10g K_3[Fe(CN)6], 100 ml H_2O) was used, which favorably etches the Cr-rich phases. Moreover, the $\gamma - \gamma'$ microstructure of isothermally brazed joints was recognized by applying the Kalling's reagent (1.5 g $CuCl_2$ + 33 mL ethanol +33 mL H_2O + 33 mL HCl), which favorably etches the γ phase. Scanning electron microscopy was applied in order to investigate the microstructure of the bonding region and EDS was used to determine the chemical composition. The patterns of XRD were obtained using the PHILIPS PW3040 diffractometer with a wavelength 1.54 Å. Primary microstructural investigations of the joint were performed using an FE-SEM. Microstructural evaluations and semi-quantitative compositional analysis were performed using the FEI-QUANTA FEG450 SEM equipped with ultra-thin window EDS.

3. Results and discussion

3.1. Microstructure characterization

Typically, the optical and SEM micrographs of the joint creat at 1100 °C for 45 min are shown in Fig. 2. As mentioned, to investigate the bonding temperature effects on the rate of isothermal solidification, Inconel 718 and GTD111 superalloys couple were TLP bonded for varying times ranging between 1 and 80 min using BNi-2 filler alloy at temperatures of 1050, 1100, and 1150 °C, respectively. As shown in Fig. 2 the bonded sample could be dissevered into four regions based on their morphologies: isothermally solidified zone (ISZ), athermally solidified zone (ASZ), diffusion affected zone (DAZ), and base metals (BM).

Fig. 3 shows the SEM in secondary electron mode of the joint made at 1050, 1100, and 1150 °C, for 15 min. It can be seen the microstructure contained centerline eutectic ingredients at all the bonding temperatures. The EDS spectrum of the phases bonded for 15 min at 1100 °C was shown in Fig. 4. In the two phases in the eutectic structure detected boron. Nickel-rich and chromium-rich borides specified in EDS analysis and a free boride phase also identified as a Ni-based γ solid solution phase. Actually, small amounts of Ni-rich silicides were made in the eutectic gamma solid solution adjacent to the boride phases. Although the presence of silicides is quite visible in the EDS results (Table 1) it means the concentration of silicon was detected from the EDS analysis; these compounds are not visible in the SEM images. The XRD spectrum from the surfaces of a fractured bond is presented in Fig. 5. The results reveal that Ni_3B, Ni_3Si, Ni_2B, and CrB are produced in the Ni matrix. The similar phases for TLP bonding accompanied BNi-2 interlayers presented by some researchers [27]. The EDS results in Table 1 verified the phases shown in Fig. 3.

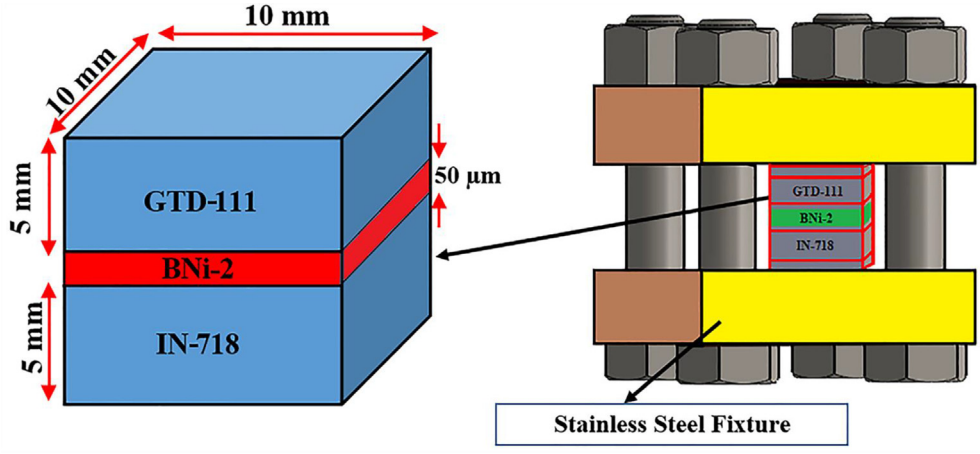

Fig. 1 – Schematic illustration of fixture for TLP bonding process.

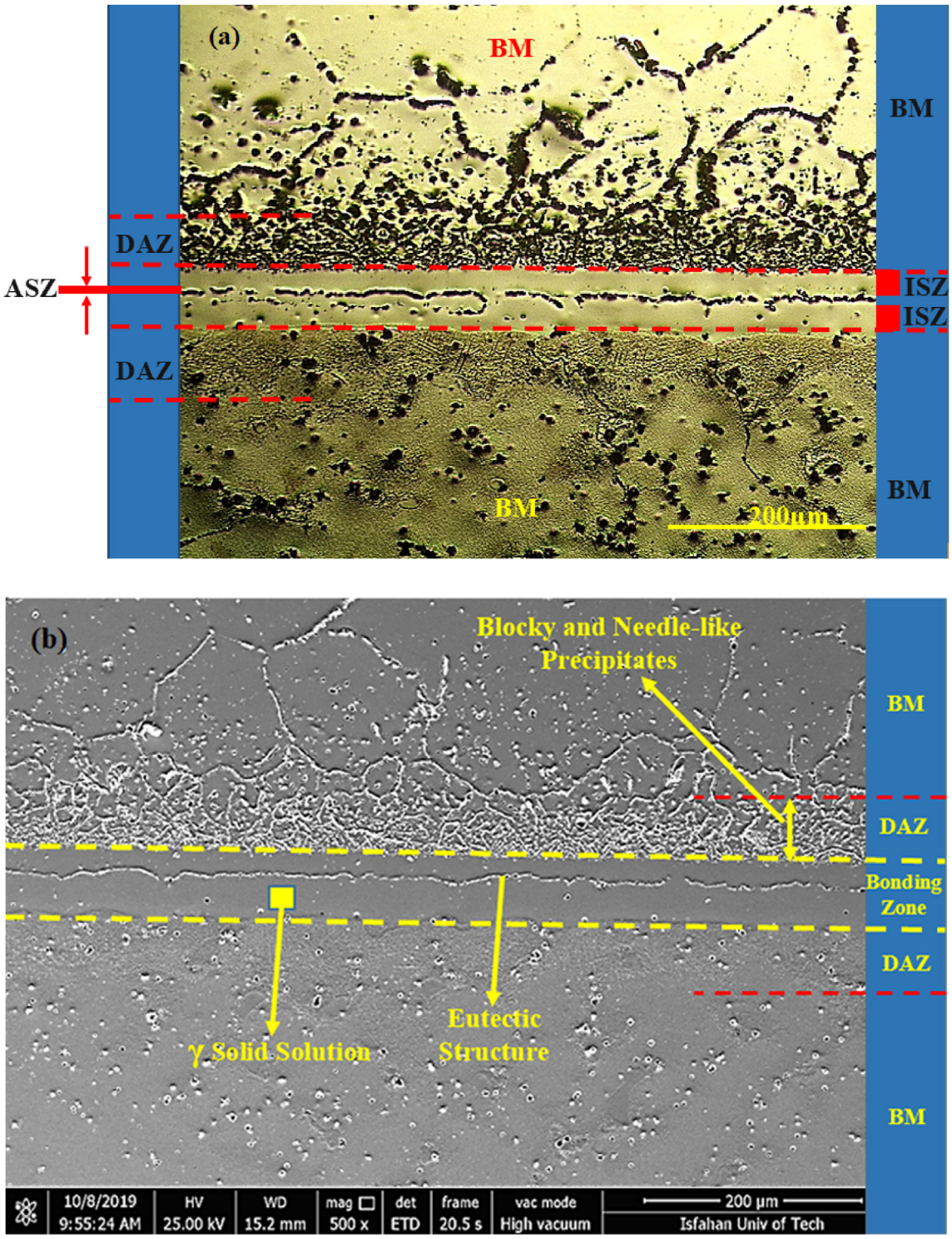

Fig. 2 – Typical micrographs of the joint made at 1100 °C for 45 min. (a) The optical, (b) SEM micrograph.

Other studies [8,9,28] dedicated such phases formed through the athermal solidification of the remaining liquid filler alloy due to incomplete isothermal solidification at the bonding temperature.

The bonding time of 15 min is not sufficient to complete isothermal solidification, but Fig. 3 shows that the increase in temperature from 1100 to 1150 °C, enhances the isothermal solidification rate. In this study, isothermal solidification was completed within 60 min at 1100 °C and after 30 min at 1150 °C, and the joints were comprised of mostly Ni-based γ-solid solution phase.

The reason for isothermal solidification completion is the increase in boron solid-state diffusion rate (as the rate-controlling factor throughout the isothermal solidification process) with bonding temperature increasing. The higher temperature above 1150 °C did not invest, but Gale et al. [29]

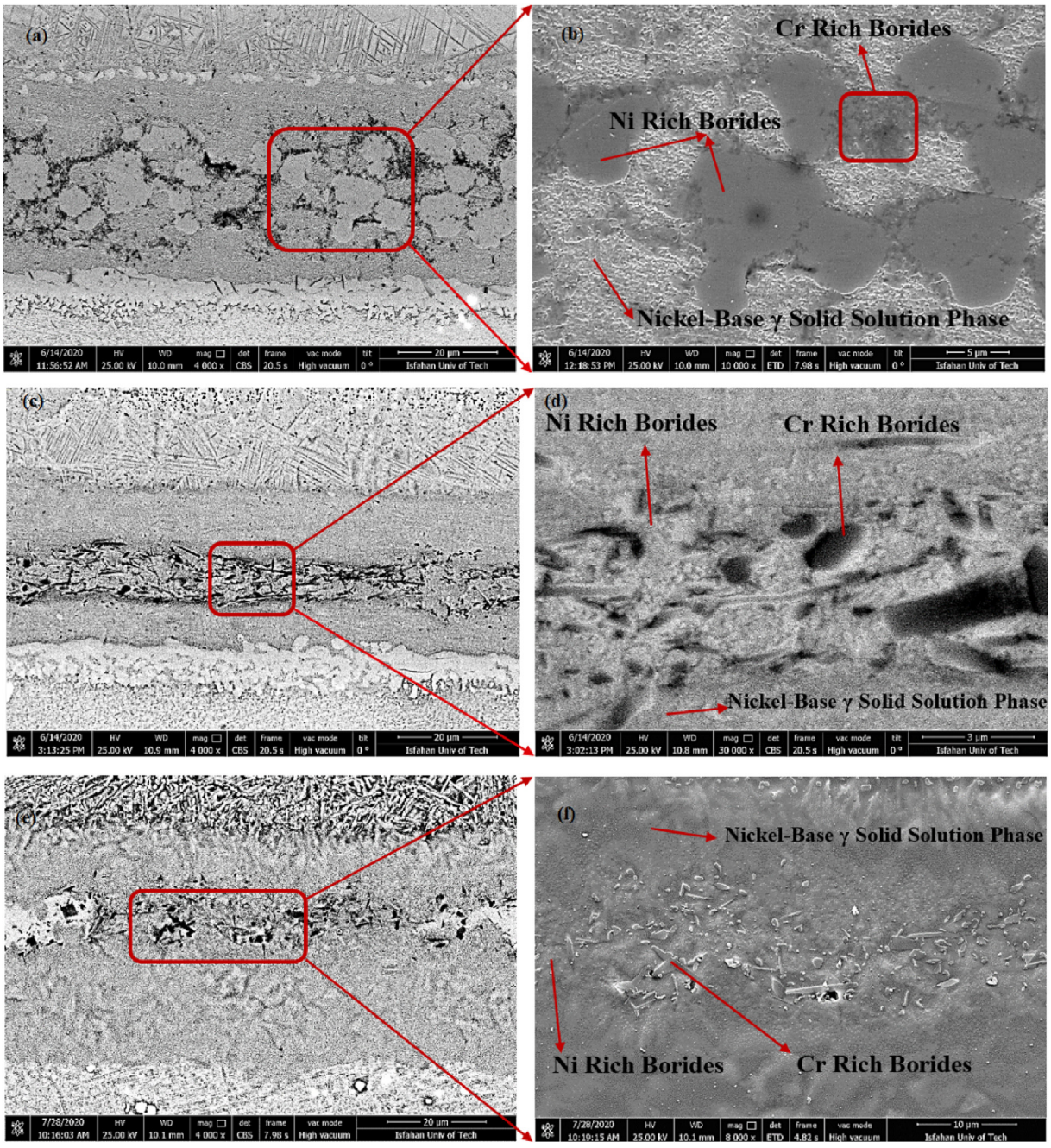

Fig. 3 – The SEM images of the joint made at 1050, 1100, and 1150 °C, for 15 min.

reported that the isothermal solidification time could reduce to a broader industrially proper level in higher temperatures, bonding carried out above 1150 °C for times surpassing the time needed for complete isothermal solidification. Some researchers [30,31] called this temperature a critical temperature. Beyond this temperature, it suppressed the formation of borides in the DAZ and developed the time required to complete isothermal solidification.

After diffusion of boron, its content decreases sharply in the centerline, and with the prolonged holding time, the liquid will be enriched approximately in silicon. When the concentration of silicon is more than the critical concentration of silicon, and when the concentration of boron is lower than the critical concentration of boron, the process of silicon diffusion becomes notable. The essential factors to control the isothermal solidification rate are initial boron and silicon concentrations in the filler metal, and they depend on boron and silicon concentrations. In this study, the time for complete isothermal solidification of liquid is high due to the high boron concentration and low silicon concentration of BNi-2. At the higher bonding temperatures, one of the significant factors for the lowering in isothermal solidification rate is the reduction in boron solubility than the increase in its diffusivity in higher temperatures. Pouranvari et al. [32] reported that TLP bonding experiments were conducted at 1100 °C using BNi-3, and BNi-2 for 20 and 25 min, respectively.

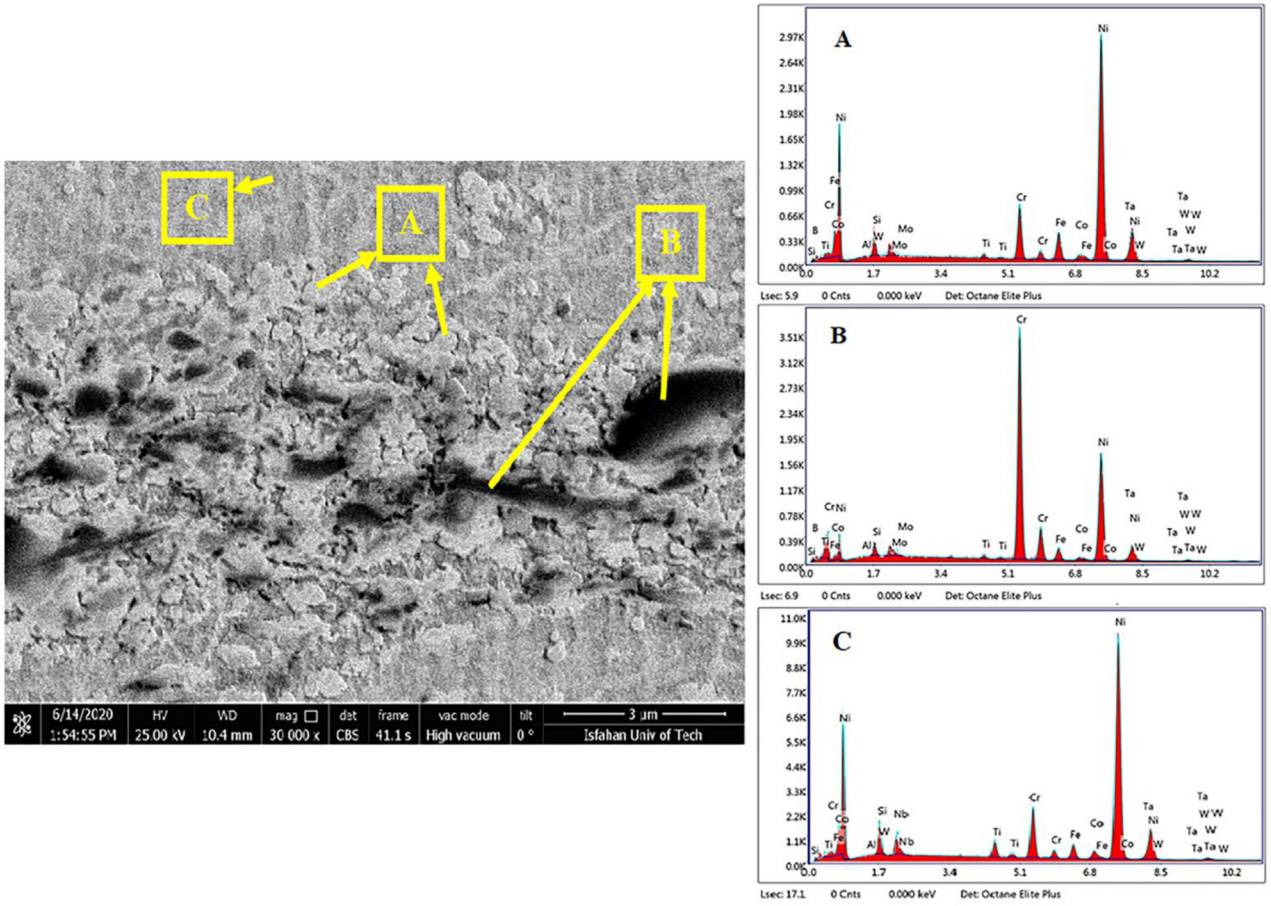

Fig. 4 – The EDS spectrum of the phases bonded for 15 min at 1100 °C.

As observed in Fig. 3, it reduced the eutectic phase's volume fraction by increasing the bonding temperature. The centerline of the joint consists of a eutectic structure, namely, athermally solidified zone (ASZ). It was made in the middle of the bonding area and contained the ternary eutectic of nickel borides and chromium borides, and some silicide particles in adjacent ISZ. Due to the solubility limit of B, Cr, and Si in nickel (0.3 at.% [33], 22 at.% [34], and 15 at.%

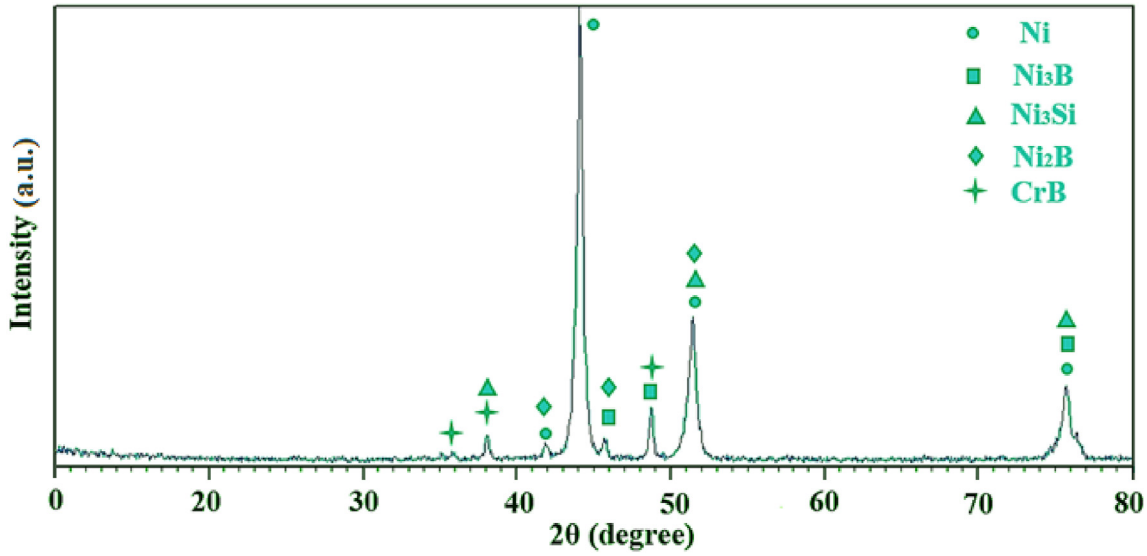

Fig. 5 – XRD pattern of the bonding region using BNi-2.

[35], respectively), the γ solid-solution formed in the ISZ region as a matrix and borides formed in the ASZ region. Dendrite morphology is the first phase that forms through cooling. Because of the low solubility of boron in Ni (0.3 at.%), it will refuse extra boron into the melted metal. The liquid will be enriched by elements such as boron that have a coefficient of distribution (k) less than unity, like Ta, Nb, Ti, and W. With the enrichment of the liquefied interlayer, alloying element concentration increases and forms the solubility limit of that element in γ. Finally, secondary phase precipitation starts between dendrites at temperatures higher than eutectic temperature. The cooling process changes the composition of the liquid and then the suspension of the solidification sequence. After that, liquid converts into γ-eutectic and Ni-rich boride (Ni_3B) following a eutectic reaction. Due to the low solubility of chromium in nickel-boride and γ-eutectic (10.11 at.% and 18 at.% respectively), chromium rejected into the liquid.

The solidification sequence is conducted for two reasons: the decrement of temperature and the Cr rejection into liquid. Concerning ternary eutectic transformation at 997 °C, melted metal converts into three phases: γ-eutectic, Ni-rich boride (Ni_3B), and Cr-rich boride (CrB). It may be observed from Table 1 that the contents of Si, which is not included in the original base metal, are 0.64%, 1.21%, 0.24%, and 7.77% in the regions of the γ-solid solution, Ni-rich boride phase, Cr-rich boride, and Ni-rich silicide respectively. Considering the measurement error, it can be observed that the contents of Si in the above-mentioned regions are identical. It means that Si distributes in the joint centerline after bonding for 15 min.

Based on the Ni–Si phase diagram [36], it is apparent that the solubility of silicon in Ni is 15 at.% above the bonding temperature range (1052–1121 °C), and hence it is awaited to have little Ni-rich silicides adjacent to the boride phases. Table 1 verified these results. It is evident that role of silicon in the microstructure development throughout TLP bonding in the standard system is lower than boron and chromium. The results showed intermetallic compounds and eutectic structure (Ni-rich and Cr-rich borides) in low temperatures and low bonding time form in the joint region during cooling. Longer bonding time or higher bonding temperature causes MPDs (Si, B) diffusion from the joint centerline to the base metal. The joint centerline's solidification chain was established to be: firstly formation of Ni-rich γ solid solution, secondly γ/Ni-rich borides, after that Cr rich borides and finally Ni-rich silicides. Such phases reported by other researchers [32].

Fig. 6 exhibits the EDS mapping of different alloying elements in the bond region and shows the partitioning function of various elements through TLP bonding. On both sides of the solidification zone were observed two diffusion-affected zones.

Fig. 7 shows SEM micrographs of DAZ on both sides of TLP bonded samples. Two types of blocky and needle-like precipitates are formed within the grains in DAZ zones. These precipitates form during a solid-state transformation. Several particles are just formed at the grain boundaries. As given in Table 2, there is a comparison between the chemical composition of needle-like precipitates and adjacent γ matrix. The IN718 superalloy's sides consisted of secondary precipitates that were enriched with Cr, Fe, Nb content. On the sides of the GTD111 consisted of secondary precipitates that revealed Cr, Mo, and Ta borides. The particles mentioned above are attributed to the MC carbides. In Ni-based superalloys, carbides are one of the principal strengthening factors. The main reasons for creating borides are the lower solubility of Boron in Ni than silicon [36] and higher diffusion coefficient of boron [37], and the strong tendency of boron to form intermetallic compounds. In lower temperatures such as 1050 and 1100 °C, the diffusion of boron is the controlling factor for the formation of intermetallic compounds in the centerline, and at the higher temperature, the diffusion of Nb in IN718 and Ti in GTD111 is the controlling factor.

3.2. *Effects of bonding temperature on completion of isothermal solidification*

To study the effects of bonding temperature on achievement of isothermal solidification, TLP bonding of GTD111/IN718 couple was carried out at different times between 1 and 80 min utilizing Ni-B-Si-Cr-Fe interlayer at varying temperatures of 1050, 1100, and 1150 °C, respectively. The rate of isothermal solidification and the ASZ width was increased by increasing the bonding temperature from 1050 to 1150 °C. Prevention from the formation of centerline eutectic constituent performed within 80 min at 1050 °C, 60 min at 1100 °C, and after 30 min at 1150 °C. The increment in the boron diffusion coefficient is the main reason for the significant reduction in the expected time to achieve a eutectic-free joint. Furthermore, as reported by other researchers, the shorter isothermal solidification time is obtained by raising the bonding temperature. The main reason for carrying out isothermal solidification is the diffusion of MPD elements such as boron and silicon outside of the liquid phase inside the substrate until the liquidus temperature of the liquid phase comes to the bonding temperature. Isothermal solidification is completed at the moment that the liquidus temperature of the remaining liquid at the heart of the joint comes to the bonding temperature. At this time concentration of MPD at the heart of the joint is decreased to the MPD solid solubility at the bonding temperature [38,39]. Accordingly, isothermal solidification time falls back on the MPD element's fluctuation from the liquid phase into the substrates and phase connection in the substrate/interlayer system. Several reasons for such multicomponent systems behavior can be pointed out as follow:

1 In lower temperatures such as 1050 and 1100 °C, the diffusion of boron is the controlling factor for the formation of intermetallic compounds in the centerline, and at the higher temperature, the diffusion of Nb in IN718 and Ti in GTD111 is the controlling factor. Ti diffusion coefficient and Nb Diffusion coefficient in Ni-based alloys are much lower than that of boron in Ni. Ti and Ni are substitutional solutes, and boron is an interstitial solute in Ni.
2 Additionally, precipitation of boride in the diffusion-affected zone can influence boron diffusion during isothermal solidification. Boron consumed fraction by boride formation and hence removed from the matrix phase enables extra boron to enter into the substrate, which affects the useful boron diffusion [40].

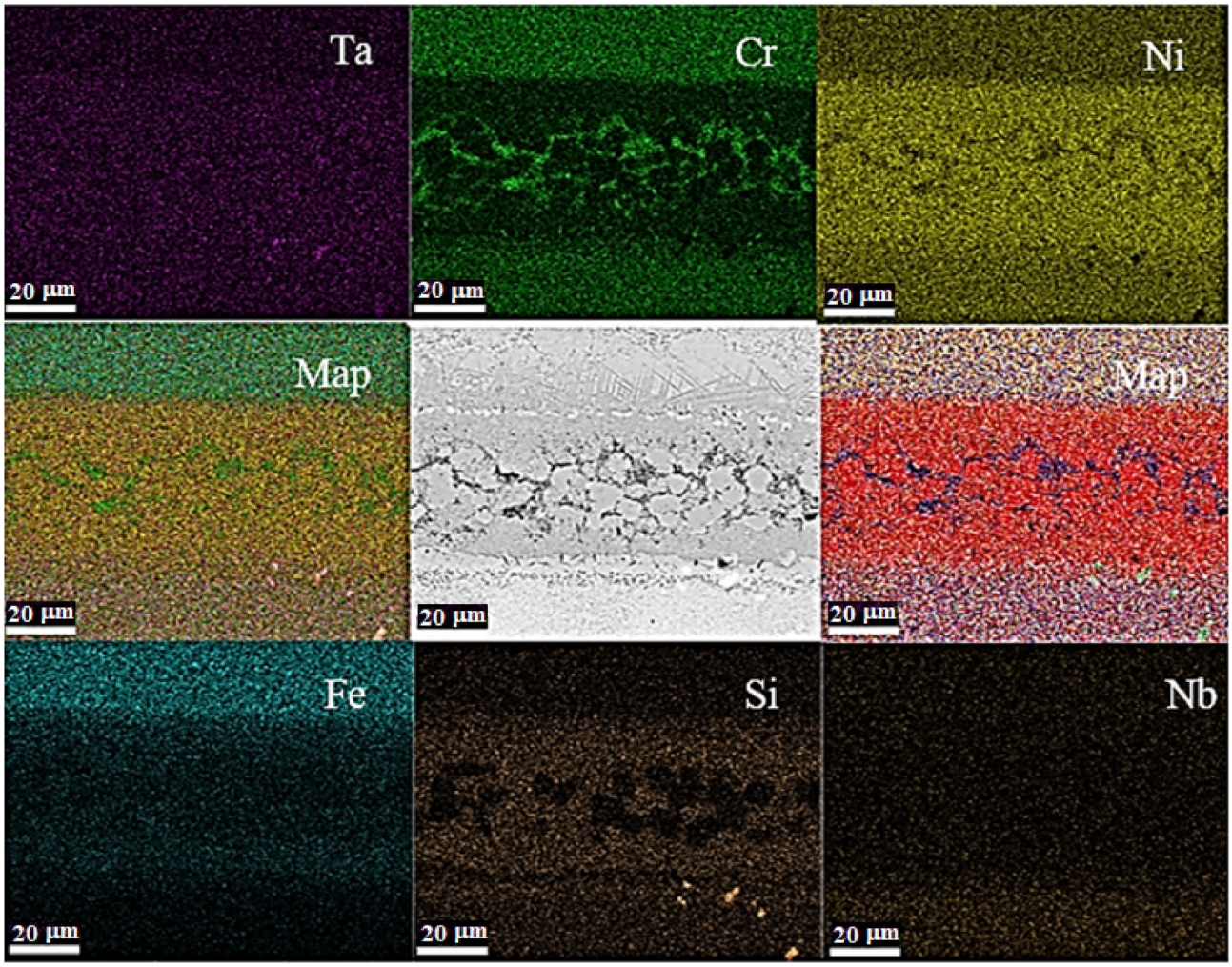

Fig. 6 – The EDS mapping of different alloying elements in bond region.

Based on Sakamoto et al.'s study [41,42], there is a linear relation between bonding temperature (T) and holding time (t). This relation is shown below:

$$(T + 20 \log t)^{½} \quad (1)$$

With increasing temperature, base metal dissolution increased, and controlling elements changed the isothermal solidification rate and reduced the B and Si element's diffusion rate from the molten interlayer into the substrates. It is worth noting that according to Fick's second law (equation (2)) [43], the shift in the concentration with time depends on the diffusion coefficient of boron and silicon elements in the substrates and concentration gradient. Increasing the diffusion coefficient and decreasing the concentration gradient related to the bonding temperature increment.

$$\frac{\partial C}{\partial t} = D\frac{\partial^2 C}{\partial X^2} \quad (2)$$

where, $\frac{\partial^2 C}{\partial X^2}$ is the concentration gradient, D is the diffusion coefficient and $\frac{\partial C}{\partial t}$ is the change in the concentration with time. Therefore, in the lower temperature (lower than 1150 °C) the influence of increasing the temperature on the diffusion coefficient increment is more important than the decrease of the concentration gradient. Hence, the isothermal solidification rate increases with increasing temperature. However, at temperatures higher than the 1150 °C, the decrease in concentration gradient is more notable than the increase in the diffusion coefficient, and consequently, enlargement of the temperature will reduce the rate of isothermal solidification.

3.3. *Effect of bonding time on completion of isothermal solidification*

Eutectic phases that form during athermal solidification has high hardness, and these brittle phases are the appropriate sites for crack initiation and consequently decrease the mechanical properties of the bond [9]. Secondary precipitates in the diffusion-affected zone, due to their discontinuous distribution at the interface of bond/substrate, have fewer harmful effects on bond strength [44]. Additionally, it is evident that there is a contrary relation between bond shear strength and ASZ size.

Fig. 8 depicts the optical microstructures of the TLP bonded joints acquired at the temperature of 1100 °C for the bonding times of 15, 30, 45, and 60 min. It was recognized that the

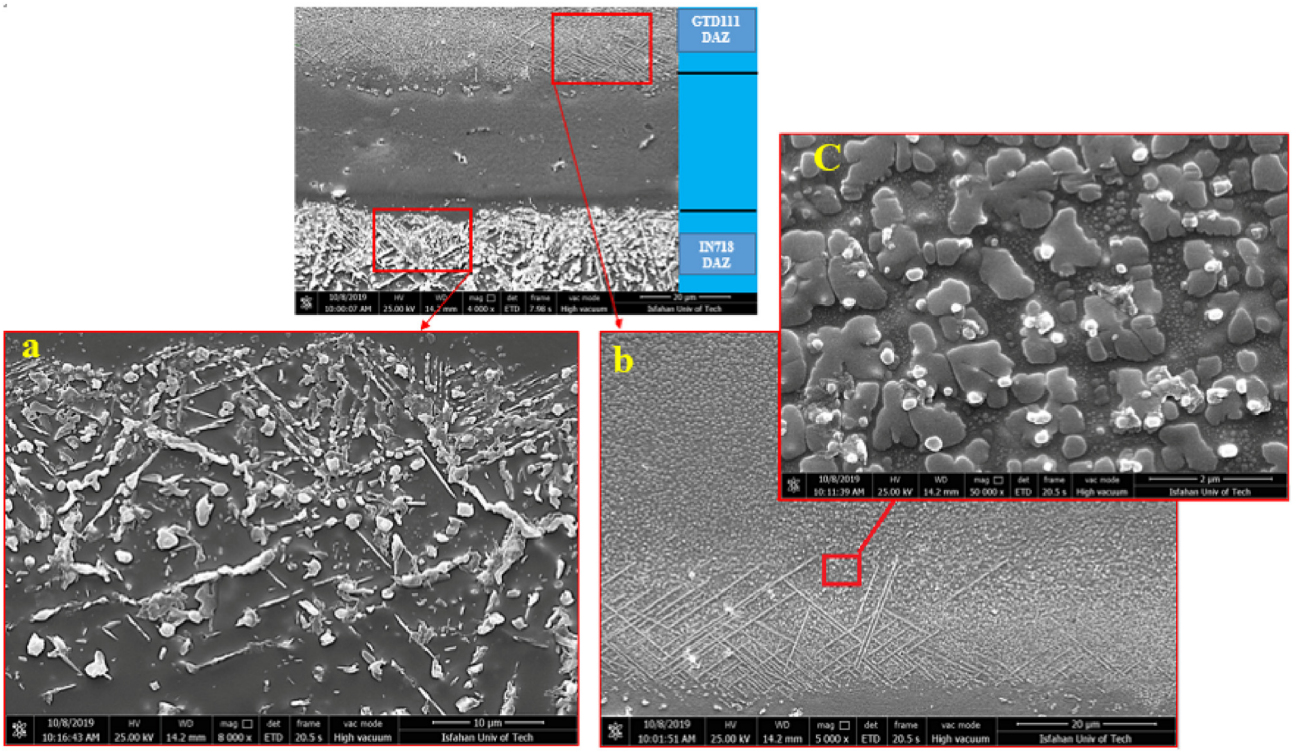

Fig. 7 – FE-SEM micrographs of the TLP bonded joint at 1100 °C for 40 min: (a) the DAZ of IN. 718, and (b) DAZ GTD111 (c) blocky shape particles.

width of the bonding zone was decreased with the increase of bonding time at the abovementioned temperature. It can be seen that the joint width decreases by isothermal solidification, and with increasing bonding time at a constant temperature, a narrow region of eutectic phases is recognized in the joint zone, indicative of complete isothermal solidification with the bonding time increasing. The joint width (size) was quantified using the image analyzing system (the error measurement in the joint width is ±3 μm). Thus, the issue is that the isothermal solidification was completed at a temperature of 1100 °C for 60 min nearly. (1) Boron flux decreasing to the base metal at the bonding temperature of 1100 °C due to the absence of boride precipitates in the base metal, and (2) enhancement of the remaining liquid with some base metal alloying elements throughout isothermal solidification and dissolution are two factors that affect on the relationship of the joint width and isothermal solidification rate. Izadi Ghahferokhi et al. [26] and Cook et al. [2] reported similar results about the relationship between bonding width and bonding time.

Intending to investigate the effect of bonding parameters on isothermal solidification progress, joining at temperatures of 1050, 1100, and 1150 °C and times of 1, 15, 30, 45, 60, and 80 min were executed. ASZ Size was calculated taking into account the eutectic and γ solid solution boundary as solid/liquid interface at any bonding time. A linear relationship between ASZ size and root of bonding time can find for other temperatures (such as 1100 and 1150 °C), and this verifies that isothermal solidification is regulated by diffusion of solid-state [32]. Other researchers developed the prediction of time required for completion of isothermal solidification and compared experimental data and analytical modeling [45–53]. Accordingly, there was a positive similarity between the outcomes of experimental and modeling data. For the reason that isothermal solidification is controlled by varying the concentration of the boron and silicon elements in the solid/liquid interface, the ASZ width is directly changed with the square root of the bonding time. As mentioned, ASZ microstructure and the solidification behavior, boron is the main controlling MPD element of

Table 2 – Chemical composition of DAZ particles (wt%); wherein blocky and needle-shaped precipitate.

Particles	Ni	Cr	Co	Ti	Al	Si	Ta
Blocky precipitates (GTD111 inside)	42.02	44.59	2.80	4.00	2.40	2.17	4.02
Needle-shaped precipitates (GTD111 inside)	13.92	59.34	8.22	7.50	3.18	1.00	7.02
Particles	**Ni**	**Cr**	**Si**	**Ti**	**Fe**	**Mo**	**Nb**
Blocky precipitates (IN718 inside)	20.12	45.29	3.28	1.81	13.61	5.11	9.60
Needle-shaped precipitates (IN718 inside)	17.96	48.58	3.81	1.90	20.35	0.99	6.43

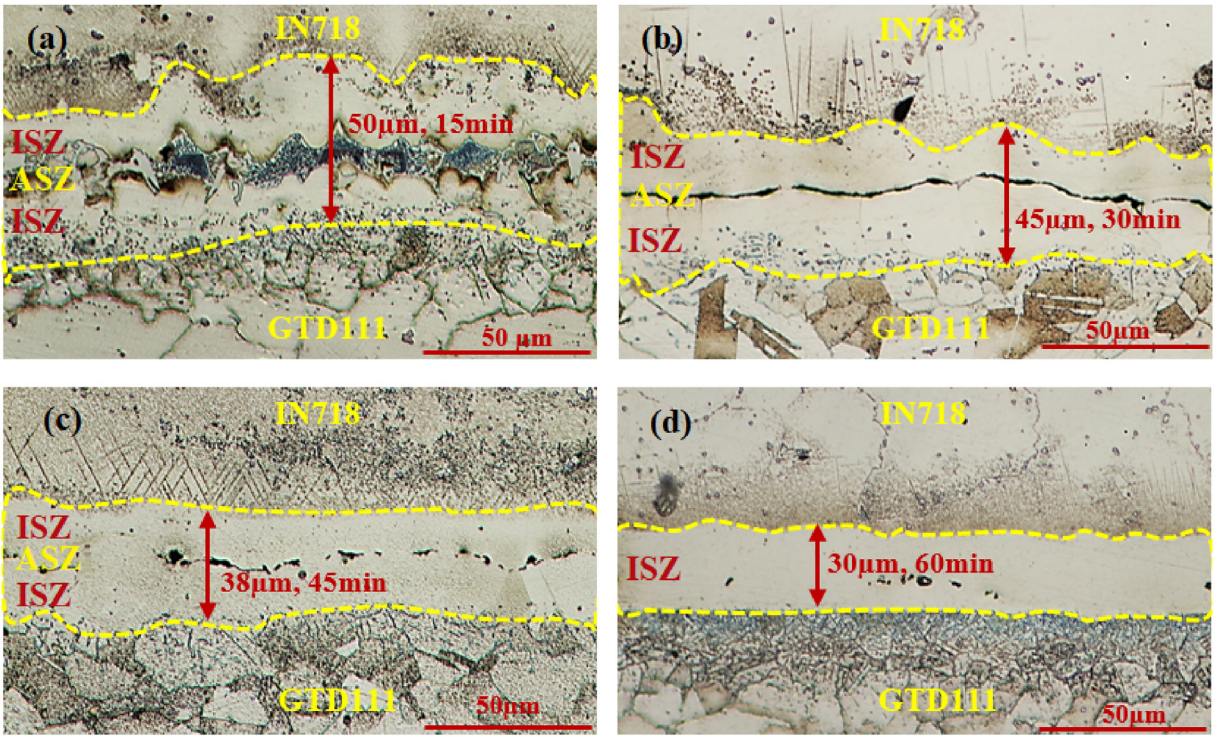

Fig. 8 – Optical microstructure of the joints made at 1100 °C for different bonding times of (a) 15, (b) 30, (c) 45 and (d) 60 min.

isothermal solidification, and silicon play no significant role in microstructure development during TLP bonding using Ni-B-Si interlayer [54–64]. As can be seen in Fig. 9, the isothermal solidification technique is dominated by the establishment and growth of γ-solid solution, which is regulated by diffusion of MPD element in substrate. The micrograph of joints at a temperature of 1100, 1050, and 1150 °C for 1–80 min shows that in lower bonding times, the microstructure contains a continuous eutectic structure in the bonding area, and by increasing the bonding time, decreases the width of the eutectic structure and consequently increased the ISZ width. Therefore, the result is that the isothermal solidification was completed at a temperature of 1050 °C for 80 min, at 1100 °C for 60 min and at 1150 °C for

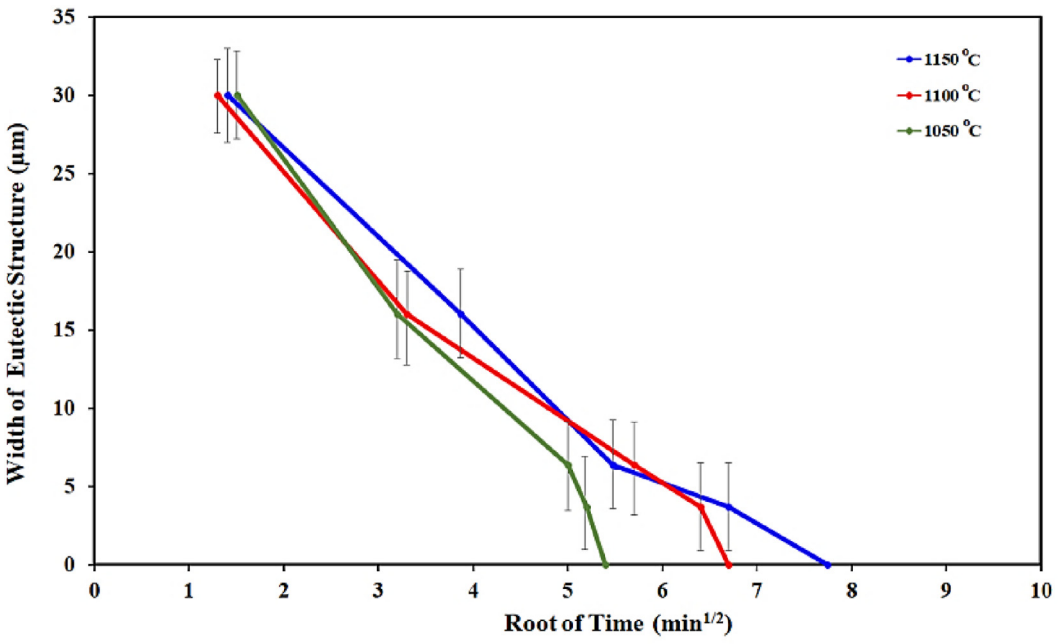

Fig. 9 – ASZ size versus square root of bonding time.

45 min. It should be noted that some regions in Fig. 9 could have overlapped with the other areas, affecting the standard deviation values.

4. Conclusions

From current research and investigation the effects of bonding temperature and bonding time on isothermal solidification rate during the transient liquid phase (TLP) bonding of GTD111/IN718 superalloys using a Ni–Cr–Si–B filler alloy. TLP process was carried out at temperatures of 1050, 1100, and 1150 °C for the holding times of 1, 15, 30, 45, 60, and 80 min. From this research, the following conclusions can be described:

1 Dissimilar joining of GTD111 to IN718 was successfully accomplished when the TLP process was performed under appropriate conditions. In addition, the microstructural investigations demonstrated that the isothermal solidification zone (ISZ) consisted of γ-solid solution and the athermally solidified zone (ASZ) consisted of Ni-rich boride phase, Cr-rich boride, and Ni-rich silicide.
2 In lower temperatures such as 1050 and 1100 °C, the diffusion of boron is the controlling factor for the formation of intermetallic compounds in the centerline, and at the higher temperature, the diffusion of Nb in IN718 and Ti in GTD111 is the controlling factor.
3 In this study successfully anticipated the time necessary for a complete isothermal solidification of the interlayer liquid in the joint centerlines at bonding temperatures of 1050, 1100, and 1150 °C. Moreover, increasing the bonding time leads to a decrease in the joint width and the formation of fewer intermetallic compounds.
4 The bonding temperature of 1100 °C for a bonding time of 60 min is recommended for the completion of isothermal solidification in GTD111/IN718 using a Ni–Cr–Si–B filler alloy. Obtaining the isothermal solidification process in higher temperatures than 1100 °C should decrease the bonding times; reaching the isothermal solidification process at lower temperatures than 1100 °C should increase the bonding times.

Declaration of Competing Interest

The authors declare that they have no known competing financial interests or personal relationships that could have appeared to influence the work reported in this paper.

REFERENCES

[1] Gale W, Butts D. Transient liquid phase bonding. Sci Technol Weld Join 2004;9:283–300.
[2] Cook GO, Sorensen CD. Overview of transient liquid phase and partial transient liquid phase bonding. J Mater Sci 2011;46:5305–23.
[3] Pouranvari M, Ekrami A, Kokabi A. Effect of bonding temperature on microstructure development during TLP bonding of a nickel base superalloy. J Alloys Compd 2009;469:270–5.
[4] Rabinkin A. Brazing with (NiCoCr)–B–Si amorphous brazing filler metals: alloys, processing, joint structure, properties, applications. Sci Technol Weld Join 2004;9:181–99.
[5] Tung S, Lim L, Lai M. Solidification phenomena in nickel base brazes containing boron and silicon. Scripta Mater 1996;34:763–9.
[6] Philips N, Levi C, Evans A. Mechanisms of microstructure evolution in an austenitic stainless steel bond generated using a quaternary braze alloy. Metall Mater Trans 2008;39:142–9.
[7] Sonawane SS, Thakur PP, Malika M, Ali HM. Recent advances in the applications of green synthesized nanoparticle based nanofluids for the environmental remediation. Curr Pharmaceut Biotechnol 2022. https://doi.org/10.2174/1389201023666220411114620.
[8] Duvall D, Owczarski W, Paulonis D. TLP bonding: a new method for joining heat resistant alloys. Weld J 1974;53:203–14.
[9] Ojo O, Richards N, Charturvedi M. Effect of gap size and process parameters on diffusion brazing of Inconel 738. Sci Technol Weld Join 2004;9:209–20.
[10] Siddiqui M, Azam MA, Ali HM. Parametric evaluation of condensate water yield from plain finned tube heat exchangers in atmospheric water generation. Arabian J Sci Eng 2022:1–21.
[11] MacDonald W, Eagar T. Transient liquid phase bonding. Annu Rev Mater Sci 1992;22:23–46.
[12] Shah TR, Ali HM, Zhou C, Babar H, Janjua MM, Doranehgard MH, et al. Potential evaluation of water-based ferric oxide (Fe2O3-water) nanocoolant: an experimental study. Energy 2022;246:123441.
[13] Sajjadi SA, Zebarjad SM, Guthrie R, Isac M. Microstructure evolution of high-performance Ni-base superalloy GTD-111 with heat treatment parameters. J Mater Process Technol 2006;175:376–81.
[14] Schilke P, Foster A, Pepe J, Beltran A. Advanced materials propel progress in land-based gas turbines. Adv Mater Process 1992;141:22–30.
[15] Uberti F, Colombo A, De Gaudenzi G, Rocchini G. Influence of temperature, sulphur dioxide and thermal exchange on deposit induced oxidation/sulphidation of alloys for fluidized bed combustors. In: In Proceedings of the Materials science forum; 1997. p. 657–64.
[16] Haafkens M, Matthey JH. A new approach to the weldability of nickel-base As-cast and power metallurgy superalloys. Weld J 1982;61:25–30.
[17] Owczarski W. Physical metallurgy of metal joining. In: Kossowsky R, Glicksman ME, editors. Metallurgical society of AIME; 1980. p. 166–90. Warrendale, PA.
[18] Silva AdC, Mei PR. Aços e ligas Especiais. 2010. 3d. São Paulo: Editora Blucher.
[19] Wang Z, Zhou D, Deng Q, Chen G, Xie W. The microstructure and mechanical properties of Inconel 718 fine grain ring forging. The Minerals, Metals and Materials Society 2010;718:343–9.
[20] Andersson J, Sjöberg GP. Repair welding of wrought superalloys: alloy 718, allvac 718plus and waspaloy. Sci Technol Weld Join 2012;17:49–59.
[21] Huang C, Wang T, Chang Y, Han W, Lee C. Tensile behaviour of different pretreated alloy 718 sheets welded with electron beam welding (EBW). Sci Technol Weld Join 2008;13:646–55.
[22] Guo H, Chaturvedi M, Richards N. Effect of sulphur on hot ductility and heat affected zone microfissuring in Inconel 718 welds. Sci Technol Weld Join 2000;5:378–84.

[23] Guo H, Chaturvedi M, Richards N. Effect of boron concentration and grain size on weld heat affected zone microfissuring in Inconel 718 base superalloys. Sci Technol Weld Join 1999;4:257–64.
[24] Madhusudhana Reddy G, Srinivasa Murthy C, Viswanathan N, Prasad Rao K. Effects of electron beam oscillation techniques on solidification behaviour and stress rupture properties of Inconel 718 welds. Sci Technol Weld Join 2007;12:106–14.
[25] Janaki Ram G, Venugopal Reddy A, Prasad Rao K, Madhusudhan Reddy G. Control of Laves phase in Inconel 718 GTA welds with current pulsing. Sci Technol Weld Join 2004;9:390–8.
[26] Ghahferokhi AI, Kasiri-Asgarani M, Amini K, Ebrahimi-kahrizsangi R, Rafiei M. Evolution of microstructure and mechanical properties on dissimilar transient liquid phase (TLP) bonding of GTD-111 and IN-718 by BNi-9 (AWS A5. 8/A5. 8M) interlayer. Welding in the World; 2020. p. 1–15.
[27] Ghahferokhi AI, Kasiri-asgarani M, Amini K, Rafiei M, Ebrahimi-kahrizsangi R. Role of interlayer composition in microstructure and mechanical properties during TLP bonding of GTD-111/IN-718 superalloys. Trans Nonferrous Metals Soc China 2022;32:908–26.
[28] Ohsasa K, Narita T, Shinmura T. Numerical modeling of the transient liquid phase bonding process of Ni using Ni-B-Cr ternary filler metal. J Phase Equil 1999;20:199.
[29] Gale W, Wallach E. Microstructural development in transient liquid-phase bonding. Metall Trans A 1991;22:2451–7.
[30] Shamsabadi AY, Bakhtiari R. TLP bonding of IN738/MBF20/IN718 system. J Alloys Compd 2016;685:896–904.
[31] Atabaki MM. Microstructural evolution in the partial transient liquid phase diffusion bonding of Zircaloy-4 to stainless steel 321 using active titanium filler metal. J Nucl Mater 2010;406:330–44.
[32] Pouranvari M, Ekrami A, Kokabi A. Diffusion induced isothermal solidification during transient liquid phase bonding of cast IN718 superalloy. Can Metall Q 2014;53:38–46.
[33] Pouranvari M, Ekrami A, Kokabi A. Phase transformations during diffusion brazing of IN718/Ni–Cr–B/IN718. Mater Sci Technol 2013;29:980–4.
[34] Nash P. The Cr– Ni (chromium-nickel) system. Bull Alloy Phase Diagr 1986;7:466–76.
[35] Khakian M, Nategh S, Mirdamadi S. Effect of bonding time on the microstructure and isothermal solidification completion during transient liquid phase bonding of dissimilar nickel-based superalloys IN738LC and Nimonic 75. J Alloys Compd 2015;653:386–94.
[36] Tokunaga T, Nishio K, Ohtani H, Hasebe M. Phase equilibria in the Ni-Si-B system. Mater Trans 2003;44:1651–4.
[37] Pouranvari M, Ekrami A, Kokabi A. Solidification and solid state phenomena during TLP bonding of IN718 superalloy using Ni–Si–B ternary filler alloy. J Alloys Compd 2013;563:143–9.
[38] Idowu O, Richards N, Chaturvedi M. Effect of bonding temperature on isothermal solidification rate during transient liquid phase bonding of Inconel 738LC superalloy. Mater Sci Eng, A 2005;397:98–112.
[39] Wikstrom N, Ojo O, Chaturvedi M. Influence of process parameters on microstructure of transient liquid phase bonded Inconel 738LC superalloy with Amdry DF-3 interlayer. Mater Sci Eng, A 2006;417:299–306.
[40] LeBlanc A, Mevrel R. High temperature materials for power engineering conference. 1990. p. 1451–60. Liege, Belgium.
[41] Sakamoto A. Optimizing processing variables in high-temperaure brazing with nickel-based filler metals. Weld J 1989;69:63–71.
[42] Ejaz F, Pao W, Ali HM. Numerical investigation and prediction of phase separation in diverging T-junction. Int J Numer Methods Heat Fluid Flow 2022. https://doi.org/10.1108/HFF-12-2021-0782.
[43] Fick A. Poggendorff's flannel. Physik 1855;94:297.
[44] Pouranvari M, Ekrami A, Kokabi A. Microstructure–properties relationship of TLP-bonded GTD-111 nickel-base superalloy. Mater Sci Eng, A 2008;490:229–34.
[45] Nakao Y, Nishimoto K, Shinozaki K, Kang C. Theoretical research on transient liquid insert metal diffusion bonding of nickel base alloys. Transactions of the Japan Welding Society 1989;20:60–5.
[46] Zhou Y. Analytical modeling of isothermal solidification during transient liquid phase (TLP) bonding. J Mater Sci Lett 2001;20:841–4.
[47] Zhou Y, Gale W, North T. Modelling of transient liquid phase bonding. Int Mater Rev 1995;40:181–96.
[48] Pekař L, Song M, Mao N, Ali HM, Wu W, Cai J. Emerging sustainable and energy-efficient technologies in heat pumps for residential heating. Front Energy Res 2022;10:866466.
[49] Naalchian M, Kasiri-Asgarani M, Shamanian M, Bakhtiari R, Bakhsheshi-Rad HR. Effect of substrate's heat treatment on microstructure and mechanical properties TLP bonding of dissimilar X-45/FSX-414 cobalt based superalloys. Met Mater Int 2021;27(11):4657–68.
[50] Gogheri MS, Kasiri-Asgarani M, Bakhsheshi-Rad HR, Ghayour H, Rafiei M, Mostafa A, et al. Friction welding of pure titanium-AZ31 magnesium alloy: characterization and simulation. Eng Fail Anal 2022;131:105799.
[51] Naalchian M, Kasiri-Asgarani M, Shamanian M, Bakhtiari R, Bakhsheshi-Rad HR, Berto F, et al. Phase Formation during heating of amorphous nickel-based BNi-3 for joining of dissimilar cobalt-based superalloys. Materials 2021;14(16):4600.
[52] Doroudi A, Pilehrood AE, Mohebinia M, Dastgheib A, Rajabi A, Omidvar H. Effect of the isothermal solidification completion on the mechanical properties of Inconel 625 transient liquid phase bond by changing bonding temperature. J Mater Res Technol 2020;9(5):10355–65.
[53] Naalchian M, Kasiri-Asgarani M, Shamanian M, Bakhtiari R, Bakhsheshi-Rad HR. Comprehensive microstructural investigation during dissimilar transient liquid phase bonding cobalt-based superalloys by BNi-9 amorphous interlayer foil. J Mater Res Technol 2021;13:2144–60.
[54] Zhang Y, Li H, Li Z. The role of liquid feeding in nugget-edge cracking in resistance spot welding of dissimilar magnesium alloys. J Mater Res Technol 2021;12:788–95.
[55] Shehabeldeen TA, Yin Y, Ji X, Shen X, Zhang Z, Zhou J. Investigation of the microstructure, mechanical properties and fracture mechanisms of dissimilar friction stir welded aluminium/titanium joints. J Mater Res Technol 2021;11:507–18.
[56] Chen G, Zhang G, Wang H, Yin Q, Huang Y, Zhang B. Effect of heat distribution on microstructure and mechanical properties of electron beam welded dissimilar TiAl/TC4 joint. J Mater Res Technol 2020;9(6):13027–35.
[57] Yu J, Zhang H, Wang B, Gao C, Sun Z, He P. Dissimilar metal joining of Q235 mild steel to Ti6Al4V via resistance spot welding with Ni–Cu interlayer. J Mater Res Technol 2021;15:4086–101.
[58] Dong KW, Kong J, Peng Y, Zhou Q, Wang KH. Thermoplastic bonding of TC4 and 316L stainless steel with a Ti-based bulk metallic glass as the filler metal. J Mater Res Technol 2021;11:487–97.
[59] Tazikeh H, Mirsalehi SE, Shamsipur A. Relationship of isothermal solidification completion and precipitate

formation with mechanical properties of Inconel 939 joints vacuum TLP bonded by an amorphous Ni–Cr–Fe–Si–B filler alloy. J Mater Res Technol 2022;18:4762–74.
[60] Zeng S, You G, Yao F, Li Q, Wang L, Cao H. Coupling effect of bonding temperature and reduced interlayer thickness on the interface characteristics and quality of the diffusion-bonded joints of Zr alloys. J Mater Res Technol 2022;18:2699–710.
[61] Zhang X, Li L, Liou F. Additive manufacturing of stainless steel–copper functionally graded materials via Inconel 718 interlayer. J Mater Res Technol 2021;15:2045–58.
[62] Gu X, Cui M, Chen J, Sun D, Gu X, Liu L. Laser welding of 6082 aluminum alloy to TC4 titanium alloy via pure niobium as a transition layer. J Mater Res Technol 2021;13:2202–9.
[63] Ebrahimi M, Liu G, Li C, Wang Q, Jiang H, Ding W, et al. Experimental and numerical analysis of Cu/Al8011/Al1060 trilayered composite: a comprehensive study. J Mater Res Technol 2020;9(6):14695–707.
[64] Singh VP, Patel SK, Ranjan A, Kuriachen B. Recent research progress in solid state friction-stir welding of aluminium–magnesium alloys: a critical review. J Mater Res Technol 2020;9(3):6217–56.